JOURNAL OF Materials CHEMISTRY

Hydrothermal synthesis of nanosized anatase and rutile TiO_2 using amorphous phase TiO_2

Hengbo Yin,[a] Yuji Wada,[a] Takayuki Kitamura,[a] Shingo Kambe,[a] Sadao Murasawa,[b] Hirotaro Mori,[c] Takao Sakata[c] and Shozo Yanagida*[a]

[a]*Material and Life Science, Graduate School of Engineering, Osaka University, Yamada-oka, Suita, Osaka 565-0871, Japan*
[b]*Cygnus Enterprise Inc., Kawara-machi Chuo-ku, Osaka 541-0048, Japan*
[c]*Research Center for Ultra-High Voltage Electron Microscopy, Osaka University, Yamada-oka, Suita, Osaka 565-0871, Japan. E-mail: yanagida@chem.eng.osaka-u.ac.jp; Fax: +81-6-6879-7875; Tel: +81-6-6879-7924*

Received 8th November 2000, Accepted 6th March 2001
First published as an Advance Article on the web 9th April 2001

Phase-pure TiO_2 nanocrystallites with narrow particle-size distributions were selectively prepared by hydrothermal processes starting from amorphous TiO_2. Autoclaving amorphous TiO_2 in the presence of HF and HCl as cooperative catalysts led to the formation of narrow-sized anatase TiO_2 with a regular crystalline surface. Use of nitric acid as a cooperative catalyst with HF also gave the anatase TiO_2 with a narrow size distribution but with a rather irregular crystalline surface. On the other hand, amorphous TiO_2 was converted to phase-pure rutile TiO_2 nanocrystallites by autoclaving in the presence of citric and nitric acids. Chelation of TiO_6 octahedra with citric acid and acidification with nitric acid are critical for the phase transition from amorphous to rutile. The shape of all rutile nanocrystallites was rod-like. The crystal growth of TiO_2 to phase-pure anatase or rutile was proposed to proceed *via* respective face-sharing and edge-sharing processes through dissolution–precipitation of the dissolved TiO_6 octahedra from the amorphous phase. The photocatalytic activity in the redox reaction of 2-propanol with oxygen was quite comparable among the synthesized anatase and rutile nanocrystallites.

Introduction

TiO_2 has three crystal phases, *i.e.*, anatase, rutile, and brookite. Anatase TiO_2 has been extensively investigated owing to its notable functions for photocatalysis and photon–electron transfer.[1,2] On the other hand, rutile is a thermodynamically stable phase possessing a smaller band gap energy (3.0 eV) than the anatase phase (3.2 eV).[3,4] In photocatalysis research, chemists have been paying much greater attention to anatase TiO_2 than to rutile TiO_2 because anatase had been considered to be more active than rutile. Recently, excellent properties of rutile TiO_2 were disclosed; Beck and Siegel reported the high photocatalytic activity for decomposition of H_2S gas,[5] and Ohno *et al.*[6] reported the high activity of rutile for photooxidation of water with Fe^{3+} as an electron acceptor. To our knowledge, however, no comparison of the photocatalysis between the nanocrystallites of rutile and anatase prepared under comparable conditions has been reported so far.

A variety of preparation methods of TiO_2 nanocrystallites have been investigated and reported. As for anatase TiO_2 nanocrystallites, hydrothermal methods using amorphous TiO_2,[7] $TiCl_4$[8–10] or $TiOCl_2$ aqueous solution,[11] and sol–gel methods using titanium alkoxides[2,12–18] are worth noting. The starting materials have a profound influence on the formation of anatase TiO_2 nanocrystallites with well-defined crystalline morphology. The presence of anionic species introduced from the starting materials affects the nucleation process,[7] the crystal growth, and the morphology.[3,9,19,20]

With regard to rutile TiO_2 nanocrystallites, there were some difficulties in identifying suitable preparation processes. Thermodynamically stable rutile can be obtained by high temperature calcination of the kinetically stable anatase phase.[15,16,18,21] However, the calcination unavoidably led to sintering of the nanocrystallites.[10,16,18] Lengthy peptization of an aqueous solution of $TiOCl_2$ gave rutile nanocrystallites, followed by coagulation giving secondary particles (200–400 nm in diameter).[11]

Interestingly, a series of recent reports suggested that hydrothermal methods under acidic conditions were applicable to the synthesis of rutile nanocrystallites, similarly to the preparation of anatase nanocrystallites. Yanagisawa and Ovenstone[7] reported that hydrothermal treatment of an amorphous TiO_2 suspension prepared beforehand by neutralization of $TiCl_4$ or by hydrolysis of $Ti(OC_2H_5)_4$ under acidic conditions using HCl (0.5 M) led to the formation of a mixture of anatase, brookite, and rutile nanocrystallites. In addition, Aruna *et al.*[22] reported the synthesis of 20 nm rutile nanocrystallites from titanium isopropoxide in the presence of nitric acid (pH 0.5) under vigorous stirring during hydrothermal treatment. Furthermore, a Japanese patent[23] claimed that cube-shaped rutile TiO_2 with an average particle size of 18 nm can be hydrothermally prepared from neutralized $TiCl_4$ suspension in the presence of citric acid.

These recent works prompted us to synthesize phase-pure anatase and rutile nanocrystallites by the hydrothermal method using amorphous TiO_2 as a starting material and various acids as catalysts. We now report that phase-pure anatase and rutile TiO_2 nanocrystallites are selectively synthesized from the amorphous phase using different kinds of acids such as HF, HCl, HNO_3, and citric acids. The photocatalytic activities of the synthesized TiO_2 nanocrystallites were compared by examining the photooxidation of 2-propanol as a model photocatalytic reaction.

 DOI: 10.1039/b008974p

Experimental

Nanosized anatase TiO_2 synthesis

Amorphous TiO_2 was prepared by the following route. $TiCl_4$ (100 ml, Ti 16.5 wt.%) (guaranteed reagent grade from Wako Pure Chemicals Industries) was diluted with ice-water (100 ml) under vigorous stirring. A 3 M Na_2CO_3 aqueous solution (326 ml) was added dropwise into the transparent $TiCl_4$ aqueous solution to obtain a white precipitate, giving a suspension of pH 10. The precipitate was washed with ion-exchanged water until the filtrate conductance was decreased to 20 mS m^{-1}. The precipitate is hereafter denoted as Am. The amorphous TiO_2 (Am) prepared as above was divided into three parts, and into each one were added hydrofluoric acid (50%) and either hydrochloric acid (36%) or nitric acid (60%) in different amounts as a cooperative acid catalyst, and ion-exchanged water to give a total volume of 250 ml. The suspension was peptized at 70 °C for 3 h and then autoclaved in a Teflon-lined autoclave at 220 °C for a given time. The peptized samples before autoclaving are denoted as A*x*p, and the peptized and autoclaved samples are denoted as A*x*, where *x* is a sample number corresponding to the various preparation conditions. The preparation conditions of the samples are listed in Table 1.

Nanosized rutile TiO_2 synthesis

For rutile TiO_2 nanocrystallite preparation, the neutralization process of $TiCl_4$ aqueous solution was similar to that mentioned for anatase TiO_2 preparation, the amounts and concentrations of reactants were: $TiCl_4$, 150 ml, Ti 16.5%; ice water, 600 ml; Na_2CO_3 aqueous solution, 1500 ml (2.1 M). After neutralization, 3.6 g (0.019 mol) of citric acid was added to the suspension under stirring, and then the citric acid-containing TiO_2 aqueous suspension was peptized at 60 °C for 1 h. The obtained precipitate was washed with ion-exchanged water until the conductance of the filtrate was reduced to 20 mS m^{-1}. The precipitate is denoted as Amc, hereafter. The precipitate (Amc) was evenly divided into three parts. Into each part were added nitric acid (60 wt.%) solution in various amounts and ion-exchanged water to a total volume of 250 ml. After aging at room temperature for 3 h, the suspension was autoclaved in a Teflon-lined autoclave at 150 °C or at 220 °C for different time. The autoclaved samples are denoted as R*x*, where *x* is a sample number corresponding to the various preparation conditions. For certifying the effect of citric acid on the crystallization process, a reference sample, denoted as A, was made in the similar method as mentioned above only without adding citric acid. The sample preparation conditions are listed in Table 2.

Characterization

TiO_2 samples were washed with ion-exchanged water and separated by filtration after the hydrothermal treatment. The crystallinity of the peptized and autoclaved precipitates was checked by powder X-ray diffraction (XRD) with a Rigaku Model Dmax 2000 diffractometer using Cu Kα radiation ($\lambda = 1.54056$ Å) at 50 kV and 150 mA by scanning at 2° 2θ min^{-1}. Scherrer's equation was applied using the (110) peak to determine the pseudo-average particle size of nanosized rutile TiO_2 to reveal the effects of the preparation parameters on the crystal growth: $D = K\lambda/(B\cos\theta)$, where K was taken as 0.9, and B is the full width of the diffraction line at half of the maximum intensity.

The morphology and the size of TiO_2 nanocrystallites were investigated by high resolution transmission electron microscopy (HRTEM) with a JEOL JEM-2010 electron microscope. At the same time, electron diffraction analysis was carried out to certify the crystal phase of the nanocrystallites. The TEM sample was prepared by dropping a TiO_2 aqueous suspension onto a copper grid covered with a thin carbon layer. The particle size distribution of TiO_2 nanocrystallites was determined by directly measuring the particle sizes on the TEM images. The average particle size of each sample was determined by using the size distribution data based on a weighted-averages method.

For checking the presence of short-range order in the XRD amorphous starting materials Am and Amc, Raman spectra were obtained by using a Perkin Elmer Spectrum GX Raman instrument.

Table 1 Preparation conditions of nanosized anatase TiO_2

Sample	HF/M	HCl/M	HNO_3/M	pH	Autoclaving time at 200 °C/h
A1				9.00	2
A2	0.12			5.44	2
A3	0.12	0.23		1.77	2
A4	0.12	0.69		0.78	2
A5	0.12	1.38		0.34	2
A6	0.12	2.76		<0	2
A7	0.12	1.38		0.34	3
A8	0.12	1.38		0.34	4
A9	0.12	1.38		0.34	10
A10	0.12		0.26	1.74	4
A11	0.12		1.58	0.30	2
A12	0.12		1.58	0.30	4

Table 2 Preparation conditions of nanosized rutile TiO_2

			Autoclaving conditions	
Sample	Starting materials	pH of suspension	Temp./°C	Time/h
A	Amorphous TiO_2 prepared in a similar method to Amc but with no citric acid	0.8	150	13
R1	Amc	0.8	150	13
R2	Amc	0.8	150	22
R3	Amc	1.09	150	22
R4	Amc	1.27	150	22
R5	Amc	1.8	150	22
R6	Amc	0.8	220	6
R7	Amc	0.8	220	13

Table 3 Photocatalytic degradation of 2-propanol to acetone using anatase and rutile nanocrystallites

Catalyst	A5	A8	A12	R2	R3	R7
Conversion (%)	63.4	68.4	57.4	44.1	54.6	31.7

Reaction conditions: 2 ml 2-propanol (10 mM) aerobic aqueous solution; TiO_2, 0.5 g l^{-1}; high pressure mercury lamp, $\lambda > 315$ nm, 500 W; irradiation time, 4 h.

Photocatalytic activity

The photocatalytic activities of the freshly prepared anatase and rutile nanocrystallites were characterized using photooxidation of 2-propanol to acetone in aerated aqueous solution as a model photoreaction. The liquid phase reaction mixtures were analyzed by gas chromatography using a fused silica capillary column (HiCap-CBP20, 25 m × 0.2 mm, Shimadzu) and a flame ionization detector. The photooxidation results are listed in Table 3.

Results and discussion

Synthesis of anatase nanocrystallites

Effects of acids. The Raman spectrum of the TiO_2 precipitate (Am) prepared by neutralization of an aqueous $TiCl_4$ solution with sodium carbonate did not show any clear spectral characteristics observed for the standard samples of pure rutile and anatase TiO_2 (Fig. 1). The XRD pattern of Am did not show any crystal characteristics (Fig. 2), which was consistent with the Raman analysis. The lack of both long-range and short-range order in the sample Am suggested that the precipitate (Am) should be amorphous TiO_2.

The amorphous TiO_2 as a precursor did not crystallize even after 3 h peptization with pH 9.0 at 70 °C when judged from XRD (Fig. 2, A1p) and the Raman spectroscopy (Fig. 1, A1p). Addition of a small amount of HF (0.12 M) into the amorphous TiO_2 suspension at the peptization process lowered its pH value to 5.44, resulting in increased XRD intensity for the peaks attributed to the anatase TiO_2 phase when compared to amorphous TiO_2 (Fig. 2, A2p). When HCl acid as a cooperative catalyst was added increasingly into the peptization system, the intensities of the anatase peaks in the XRD pattern were increased, but the amorphous phase still remained

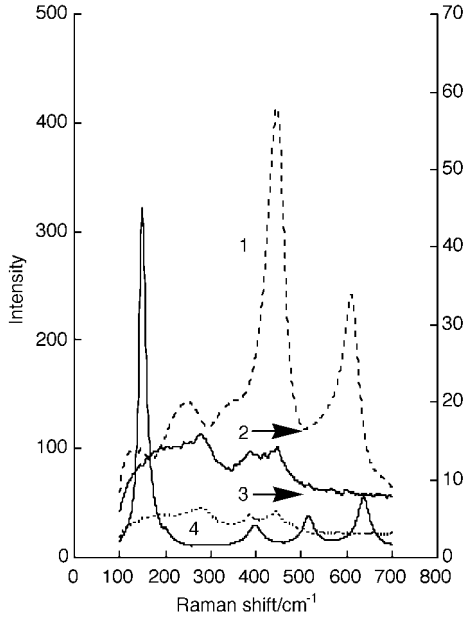

Fig. 1 Raman spectra of TiO_2: (1) pure rutile TiO_2, (2) Am, (3) A1p, and (4) pure anatase TiO_2.

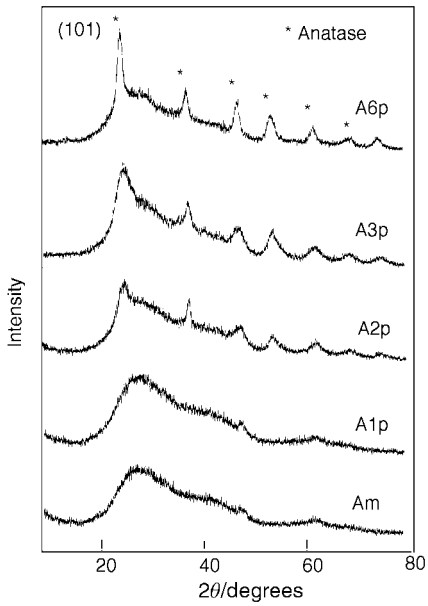

Fig. 2 XRD patterns of Am and the peptized TiO_2 samples A1p, A2p, A3p and A6p.

to a large extent after peptization at 70 °C for 3 h (Fig. 2, A3p and A6p).

When autoclaving was carried out at 220 °C in the presence of HF, the crystallization to the anatase phase from the amorphous was greatly enhanced as demonstrated by the increase of the anatase peak intensities and the decrease of the amorphous phase in the XRD patterns (A1 and A2 in Fig. 3). Interestingly, the presence of HCl with HF (Fig. 3) greatly promoted the crystallization of TiO_2 from the amorphous phase as shown by the remarkable decrease of the amorphous phase after the autoclaving. In particular, the high HCl concentration enhanced the crystallization of pure anatase TiO_2 from the amorphous phase (A5, 1.38 M (pH 0.34) and A6, 2.76 M (pH < 0)). However, under mild HCl conditions (A3, 0.23 M (pH 1.77) and A4, 0.69 M (pH 0.78)), the crystallization proceeded slowly with the formation of a small amount of rutile TiO_2. This fact was consistent with the observation by Yanagisawa and Ovenstone,[7] that the autoclaving (250 °C, 5 h) of amorphous TiO_2 in the presence of 0.5 M HCl resulted in the formation of a mixture of anatase, brookite, and rutile.

When the hydrothermal reaction temperature was maintained at 220 °C, the prolonged autoclaving enhanced selective crystal growth of anatase TiO_2 as seen in the decreased broadening of the XRD anatase peak of the 3 h autoclaved sample A7 compared to the 2 h sample A5 (Fig. 3 and 4). After 4 h autoclaving at 220 °C, the pure anatase phase prevailed (Fig. 4, A8). When the autoclaving time reached 10 h, however, a small amount of rutile TiO_2 was formed (Fig. 4, A9).

Nitric acid was found to work as a cooperative acid catalyst as well as HCl. The XRD pattern of the sample A11 (Fig. 5) showed that the formation of anatase TiO_2 from the amorphous phase was enhanced by the presence of HNO_3 when compared to that of sample A2 (with no addition of HNO_3) (Fig. 3). The broad background attributed to the amorphous phase was observed in the XRD pattern (Fig. 5, A11), indicating that a trace amount of amorphous TiO_2 still remained. At the increased HNO_3 concentration, the amorphous phase tended to decrease as seen in the XRD patterns of the samples A10 and A12 (Fig. 5).

Morphology of anatase TiO_2 nanocrystallites. Fig. 6 shows the TEM images of the prepared anatase TiO_2 samples. Sample A1, which was prepared after the peptization and autoclaving of the amorphous TiO_2 (Am) suspension at pH 9, appeared to

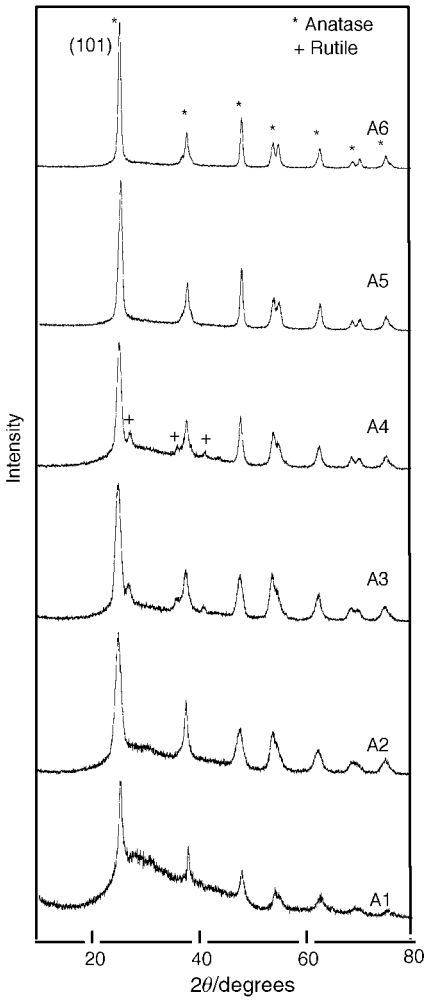

Fig. 3 XRD patterns of TiO_2 prepared from amorphous TiO_2 after peptization and autoclaving.

consist of nanocrystallites of anatase TiO_2 covered by a shell of amorphous TiO_2, and the anatase nanocrystallites were irregularly shaped. When the TEM technique was used to examine the crystalline structure of the formed nanocrystallites, the electron diffraction pattern veriified that only the anatase phase was present. A large size distribution was observed ranging from 1 to 21 nm, which gave an average size

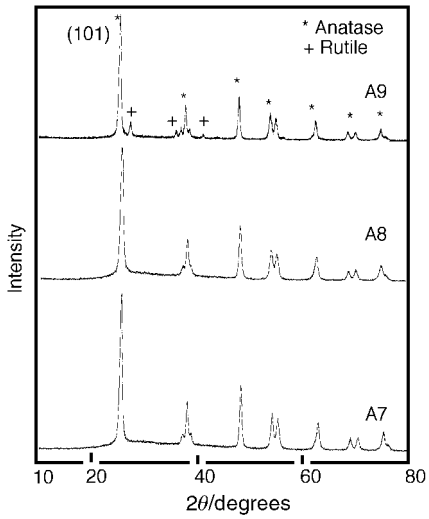

Fig. 4 XRD patterns of TiO_2 at different autoclaving times with HF and HCl as cooperative acid catalyst.

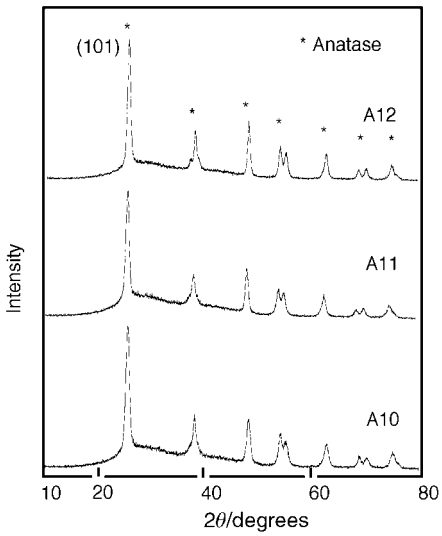

Fig. 5 XRD patterns of TiO_2 samples after peptization and autoclaving with HF and HNO_3 as cooperative acid catalysts.

of 11 nm (Fig. 7, A1). The broad particle size distribution suggested that crystallization to the anatase structure from the amorphous phase should be a solid-state epitaxial crystal growth with a slow nucleation process.

For the anatase TiO_2 nanocrystallites prepared using HF and HCl as cooperative acid catalysts, TEM images show their clear cube-like geometry, *i.e.* the nanocrystallites have regularly exposed surfaces (Fig. 6, A5 and A8). Fig. 7 shows that the particle size distributions are in the ranges from 5 to 15 nm and from 9 to 20 nm with average sizes 9 and 13 nm for samples A5 and A8, respectively.

When nitric acid was employed as a cooperative acid catalyst with HF, TEM images show that the resulting TiO_2 samples (A10 and A12) are granular nanocrystallites with irregular surfaces when compared to the anatase TiO_2 nanocrystallites prepared using HCl as a cooperative catalyst with HF (Fig. 6, A5 and A8). Fig. 7 shows that the ranges of the size distributions and the average sizes of the anatase TiO_2 samples A10–A12 are 5–21, 11; 3–17, 9; and 6–20, 12 nm, respectively. Highly acidic conditions (A12) gave large-sized nanocrystallites with the narrow particle size distribution maintained compared to the less acidic conditions (A10). Prolonging the autoclaving time also increased the average particle size while retaining a narrow size distribution.

Synthesis of rutile nanocrystallites

Chemical structure of sample Amc. Raman spectroscopy was used to investigate the starting amorphous sample Amc to check for the presence of short-range order in this precursor. Strong fluorescence was observed in the Raman spectra only for sample Amc before and after peptization at 60 °C. This fluorescence should be caused by the organic substrate from citric acid which covered the surface of the precipitated TiO_2. Accordingly, Raman spectroscopy could not ascertain whether or not the sample Amc was short range ordered. With no addition of citric acid, the precipitated TiO_2 was pure amorphous phase with neither short nor long range order, which was confirmed by the Raman and XRD spectra. The XRD pattern of the peptized Amc (Fig. 8, Amc-p) also showed amorphous characteristics. We therefore concluded that the sample Amc before and after peptization was in an amorphous state.

Effect of citric acid. Samples R1 and A were prepared *via* the same route except that citric acid was used as an additive during the peptization process for sample R1 and not for

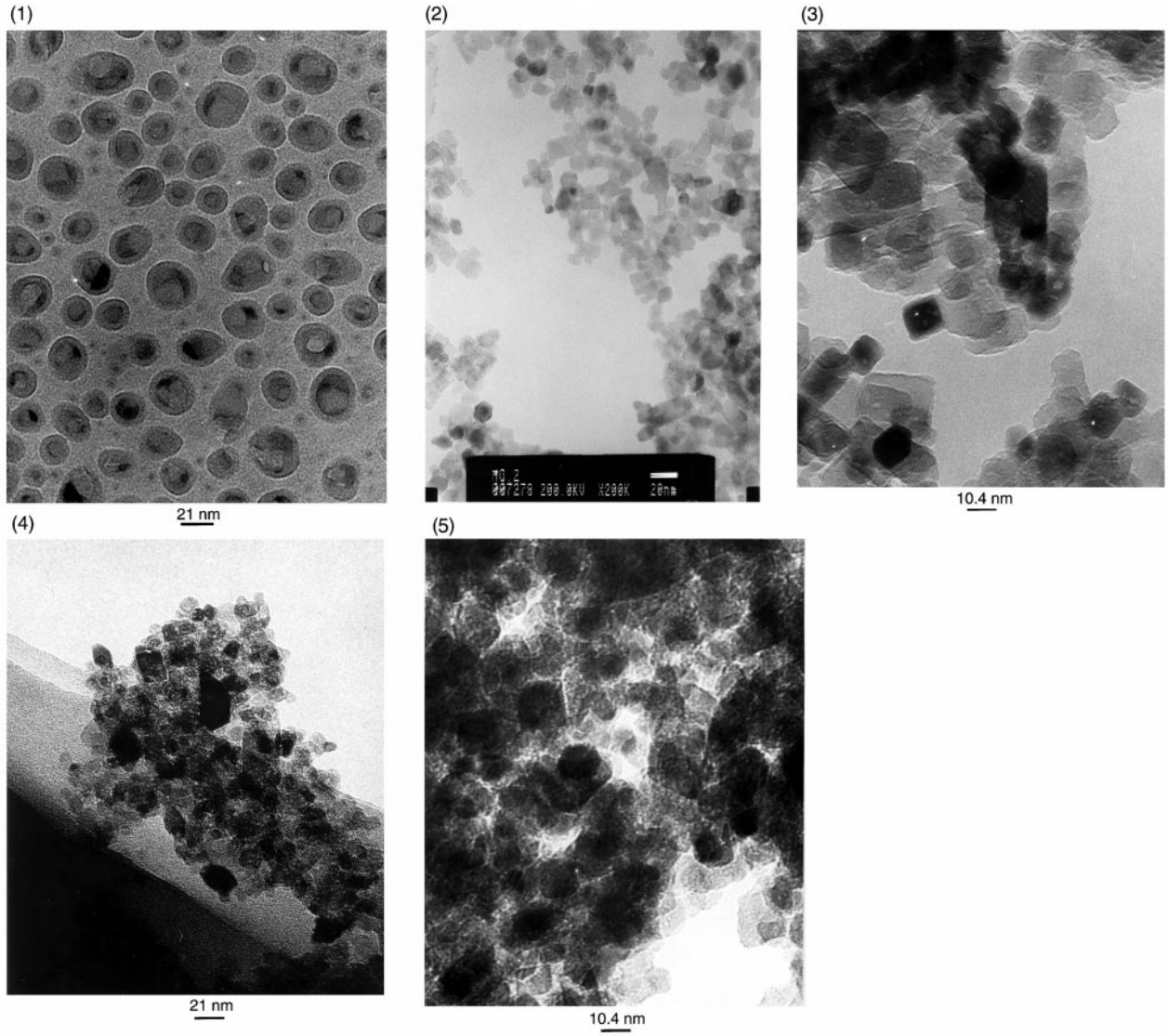

Fig. 6 TEM images of nanosized anatase TiO_2: (1) A1, (2) A5, (3) A8, (4) A10, and (5) A12.

sample A. After autoclaving at 150 °C for 13 h, the chemical structures of both samples were intrinsically different from each other. Sample R1 was a pure rutile phase, while sample A was a pure anatase phase (Fig. 8). The crystallization process of anatase from amorphous TiO_2 was postulated to proceed by face-sharing polycondensation of the protonated TiO_6 octahedra due to acid catalysis.[7] The present work revealed that a small amount of citric acid could promote phase-pure rutile rather than anatase formation. It is well known that organic additives, such as polyethylene glycol (PEG),[24,25] and surfactants,[26] in TiO_2 colloids can prevent the agglomeration of freshly formed nanoparticles during hydrothermal and calcination treatments because the additives located at the surface of the particles act as dispersing agents. However, no researchers have ever reported an interaction between citric acid and colloidal TiO_2 nanoparticles and the resulting amorphous to rutile phase transition until now.

Tsay *et al.*[27] investigated the interaction of citric acid with barium and titanium ions in barium–titanium citrate using FT-IR and ^{13}C-NMR. They found that the central deprotonated alcoholic ligand and dissociated carboxylic acid groups of citric acid chelated titanium and barium ions. It was also reported that more than 60% of the surface hydroxy groups of nanosized TiO_2 (P-25) were acylated by 2,3,4,5,6-pentafluorobenzoyl chloride or 2,3,4,5-tetrafluorophthalic anhydride.[28] Hence the exclusive formation of rutile phase in the presence of citric acid could be explained as being due to the prevention of surface-sharing polycondensation through the chelation of citrates to TiO_6 octahedra. The chelation should be beneficial to the edge-sharing rather than the face-sharing polycondensation between TiO_6 octahedra probably owing to the spatial inhibition effect of the organic ligands, giving rise to the formation of the rutile phase.

Effect of pH. Fig. 9 shows that at low pH values of the reaction suspensions (R2 pH 0.8, and R3 pH 1.09), the phase-pure rutile TiO_2 was formed after autoclaving at 150 °C for 22 h. The average particle sizes of samples R2 and R3 were estimated by Scherrer's equation to be 16.4 and 13.1 nm, respectively. It is clear that the phase-pure rutile TiO_2 with a larger particle size was formed at lower reaction suspension pH. When the pH of the reaction suspension was higher than 1.09, both anatase and rutile phases were formed concurrently and the proportion of the anatase phase was increased with increasing pH as demonstrated by the increase of the ratio of the XRD anatase peak (101) intensity to the rutile one (110) (R4 pH 1.27, R5 pH 1.80). From the XRD spectrum of sample R5, a broad background was observed and the broadening of the XRD peaks of anatase (101) and rutile (110) phases was also noted, implying the presence of unconverted amorphous phase and poor crystal growth at pH 1.27–1.80.

The effect of pH on the phase transition and crystal growth explains that the TiO_6 octahedra could be separated well by protonation at low pH and the resulting enhancement of the

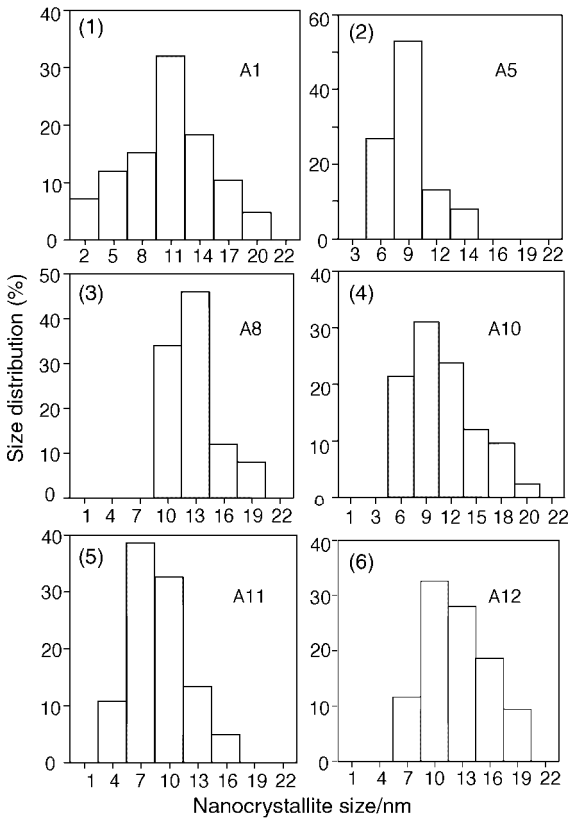

Fig. 7 Size distribution of nanosized anatase TiO_2: (1) A1, (2) A5, (3) A8, (4) A10, (5) A11, and (6) A12.

mobility of TiO_6 octahedra should be beneficial to the formation of larger crystallites by depositing the discrete TiO_6 octahedra on the preformed nuclei. On the other hand, at higher pH values, the amorphous TiO_2 could not be separated well due to less protonation, and TiO_6 units would be still in the aggregate form *via* hydrogen bonding. The aggregated amorphous TiO_2 alone should be able to take part in face-shared bonding *via* a solid-state epitaxial process during hydrothermal treatment.[7,18] The chelation of citrate to amorphous TiO_2 should be affected by the degree of protonation. If the acidity of the suspension is high enough to achieve a discrete dispersion of TiO_6 octahedra, the amorphous phase can be uniformly modified with citrate, giving rise to the formation of the pure rutile phase. Otherwise,

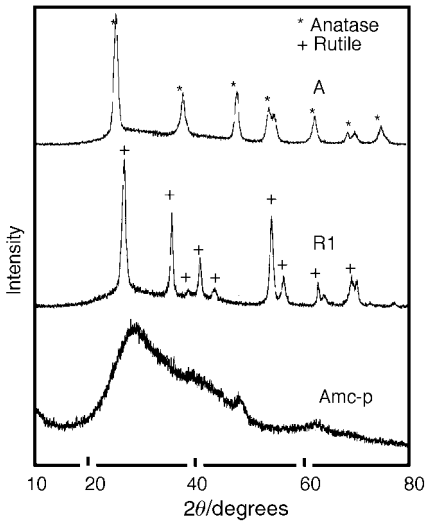

Fig. 8 XRD patterns of peptized Amc (Amc-p) and TiO_2 samples prepared with (R1) or without (A) citric acid from amorphous TiO_2.

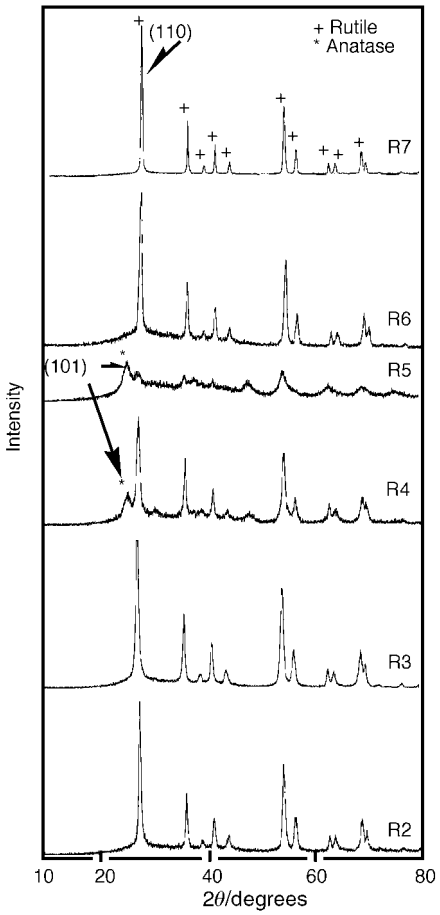

Fig. 9 XRD patterns of TiO_2 samples prepared from amorphous TiO_2 at different pH and different autoclaving temperatures and times in the presence of HNO_3 and citric acids.

the chelation of citrate to amorphous TiO_2 might be incomplete due to the existence of aggregated amorphous masses, resulting in the formation of mixed phases of rutile and anatase. The cooperative effect of nitric and citric acids on the nucleation plays a critical role in the synthesis of phase-pure rutile TiO_2 nanocrystallites using amorphous TiO_2 as a starting material.

The TEM images of samples R2 and R3 (Fig. 10) show that the morphologies of rutile nanocrystallites in both samples are rod-like. The crystallite sizes of samples R2 and R3 were 10–25×10–110 and 7–18×12–50 nm, respectively (Fig. 11). The average sizes of samples R2 and R3, calculated by a weighted-averages method, were 15×53 and 12×31 nm, respectively. In addition, the TEM images of samples R2 and R3 show that even the smaller nanocrystallites also exhibit uniaxial morphology. The crystal growth of rutile TiO_2 should be an uniaxial process under the present conditions.

The TEM images also clearly show that the aggregates (secondary particles), as denoted by the circles in the TEM image of sample R2, were constructed by oriented combination of several to several tens of primary crystallites at low pH, and the aggregation was much more obvious for sample R2 than for sample R3 which was prepared at high pH.

Effects of autoclaving temperature and time. The crystal sizes of samples R1 and R2 were 11.4 and 16.4 nm based on Scherrer's equation; samples R1 and R2 were prepared by autoclaving at 150 °C for 13 and 22 h, respectively. When the autoclaving temperature was 220 °C, the crystal sizes of samples R6 and R7 autoclaved for 6 and 13 h, respectively, were estimated to be 18.6 and 26.2 nm by Scherrer's equation.

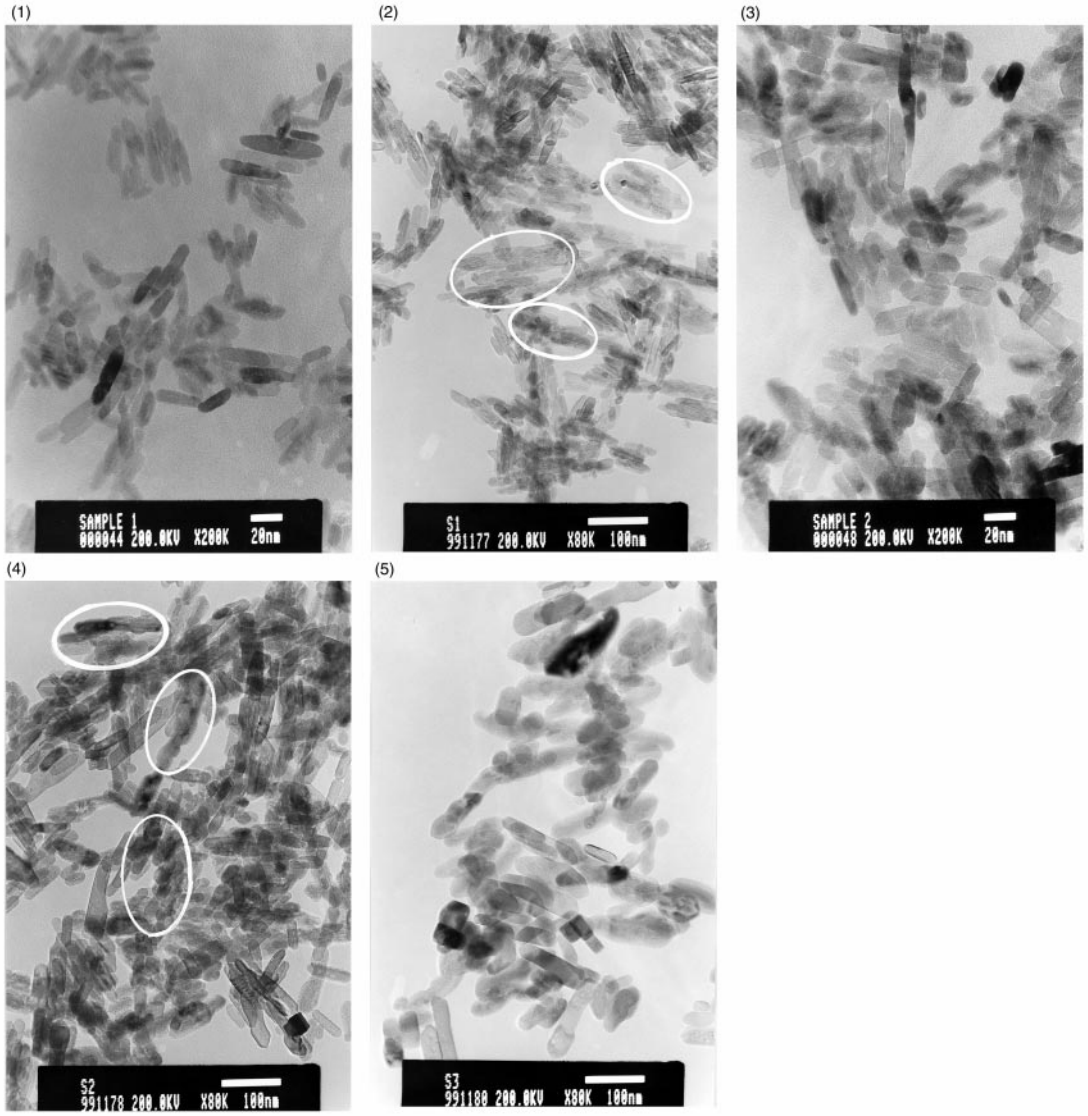

Fig. 10 TEM images of rutile TiO_2 samples hydrothermally prepared from the amorphous phase. (1) R1, (2) R2, (3) R3, (4) R6, and (5) R7.

The pH and the compositions of the reaction suspensions were all the same for R1, R2, R6, and R7. Hence it could be concluded that crystallization was promoted by increasing the autoclaving temperature and time under the present experimental conditions.

The TEM images of samples R1, R6, R7 (Fig. 10) show that the rutile nanocrystallites are rod-like and the particle size ranges are $5–12 \times 12–50$, $13–40 \times 15–140$, and $15–50 \times 20–150$ nm in width and length, respectively (Fig. 11). The average particle sizes of R1, R6, and R7 were determined to be 9×26, 22×60, and 32×73 nm, respectively. The increasing tendency of crystal growth with increasing autoclaving time and temperature observed by TEM analysis was consistent with that obtained by the XRD analysis, *i.e.*, the higher temperature and longer time of autoclaving were beneficial to the crystal growth.

Under the present experimental conditions, the minimum crystal size was >5 nm and was essentially increased with increasing autoclaving time and temperature. The nucleation process should end early in the hydrothermal process due to the acid catalysis of the polycondensation of TiO_6 octahedra.

The rutile TiO_2 has a tendency to coagulate at longer reaction times (see the TEM images of R1 and R2). The TEM image of R6 clearly demonstrates that some large (secondary) particles, as denoted by circles, are formed. The TEM image of R7 shows that the secondary particles are large rutile crystallites with the elongated shape retained.

Mechanism of anatase and rutile phase formation

Mechanism of anatase crystallization. Bahnemann *et al.*[29] described the surface acidic and basic properties of TiO_2 as follows:

$$\text{for pH} < 3.5,\ TiO_2 + n\mathrm{H}^+ = TiO_2\mathrm{H}_n^{n+}$$

$$\text{for pH} > 3.5,\ TiO_2 + n\mathrm{OH}^- = TiO_2(\mathrm{OH})_n^{n-}$$

The charge of the TiO_2 surface may be changed by such chemisorption.

On the other hand, it is known that both anatase and rutile TiO_2 can grow from TiO_6 octahedra, and that the phase transition proceeds by the rearrangement of the octahedra. Arrangement of octahedra and related species through face-sharing initiates the anatase phase, while the edge-sharing leads to the rutile phase.[7] In the present research, HCl, HNO_3 and HF acids should disperse the aggregated TiO_6 octahedra and the related species in the amorphous phase into discrete TiO_6 octahedra by protonation of the surface Ti–OH groups giving $Ti–OH_2^+$.[7,30] These protonated surfaces easily combine with –OH groups of other TiO_6 octahedra to form Ti–O–Ti oxygen bridge bonds by eliminating a water molecule. The protonation process followed by the face-sharing (Scheme 1) will result in

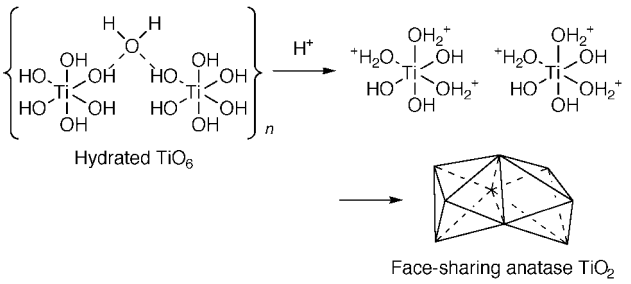

Scheme 1

the favorable formation of anatase phase from the TiO_6 octahedra.

The anions of HF, HCl, and HNO_3 exhibit different effects on the crystallization of TiO_2 from the amorphous phase according to the experimental results. Fluoride anion in aqueous HF solution should be strongly hydrated by water molecules, and have a very poor nucleophilicity. Since the fluoride anion should have no effective influence on the nucleation and crystal growth of TiO_2, the effect of protonation should prevail in the crystallization process when HF is used as a catalyst.

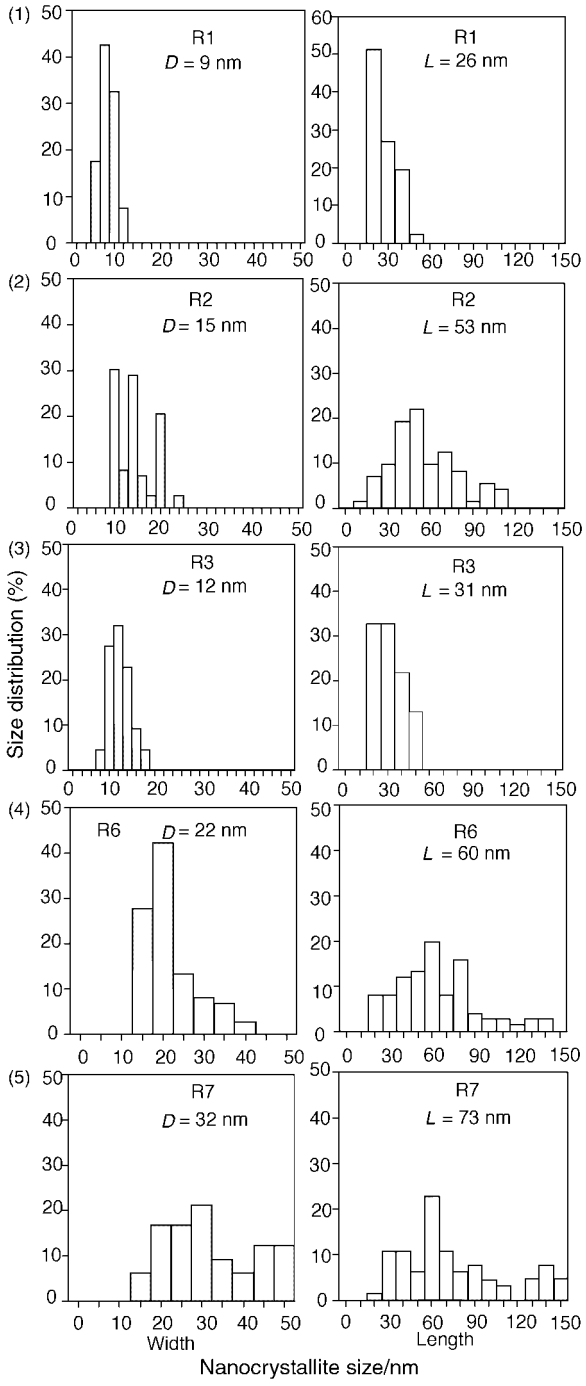

Fig. 11 Size distribution of nanosized rutile TiO_2. (1) R1, (2) R2, (3) R3, (4) R6, and (5) R7. *D* and *L*: average width and length of nanocrystallites.

Yanagisawa and Overstone[7] confirmed that the chloride anion enhances only the nucleation of anatase, not the crystal growth. Considering the uniform crystal growth and the narrow size distribution in the cooperative HF/HCl system (A5 and A8), the nucleation of anatase should be much faster than the crystal growth, ending at the early stages of the hydrothermal process when HCl is used as a cooperative catalyst. The crystal ripening should be a process in which the soluble TiO_6 octahedra and related species are precipitated with retention of the face-sharing on the surface of the existing anatase TiO_2 nuclei. In fact, the crystal size was increased when the autoclaving time was increased from 2 to 4 h and no embedding of small crystallites within the large ones was identified by TEM images when HCl was present in the system.

The broader size distribution and the presence of amorphous TiO_2 in the case of nitric acid may be ascribed to slow nucleation compared to the case of HCl. It is evident that the catalytic activity of nitric acid for anatase crystallization from the amorphous phase is lower than that of HCl. The nitrate anion has poor nucleophilicity as well as the fluoride anion, leading to the slow dispersion of the amorphous aggregates into discrete TiO_6 octahedra and related species. The slow nucleation may induce the competitive crystal growth, leading to the irregular surfaces of the anatase TiO_2 nanocrystallites.

The usage of low HCl acid concentrations of 0.23 and 0.69 M (A3 and A4) and 10 h autoclaving (A9) at a high HCl concentration of 1.38 M led to the formation of a small amount of rutile TiO_2 along with a large amount of anatase TiO_2. The competitive formation of the chloride atom-substituted octahedra similar to the partially hydrolyzed $(Ti(OH)_nCl_m)^{2-}$ species, which might be produced by the nucleophilic substitution of the chloride anion to the TiO_6 octahedra and related species like $TiO_2(OH)_n^{n-}$, may explain the slow formation of the rutile phase, since Cheng *et al.*[8] reported that the rutile phase is formed from the partially hydrolyzed complex of $TiCl_4$, *i.e.*, $(Ti(OH)_nCl_m)^{2-}$, where $n+m=6$, and that more Cl^- in the complex should be beneficial to the formation of the rutile phase.

Mechanism of rutile crystallization. The crystallization process of the rutile TiO_2 nanocrystallites under the present conditions may be depicted as shown in Scheme 2. Chelation of citrate to the TiO_6 octahedra is a decisive factor for rutile phase formation due to the spatial effect beneficial to the edge-sharing polycondensation between TiO_6 octahedra. The high degree of protonation of the TiO_6 octahedra enhanced their dispersion in favor of chelation of citrate to TiO_6 octahedra for the formation of the rutile phase and prevented the formation of the anatase phase caused by aggregation of the TiO_6 octahedra in the absence of chelation by citrate or a lower degree of protonation. The primary rutile nanocrystallites were formed by deposition and growth of the dissolved discrete TiO_6 octahedra on the existing nuclei. Further crystal growth mainly proceeded *via* oriented coalescence of the primary small grains at high autoclaving temperature and after prolonged autoclaving. The phase-pure rutile TiO_2 nanocrystallites uniaxially grew in both primary and secondary crystallite growing processes under the present conditions.

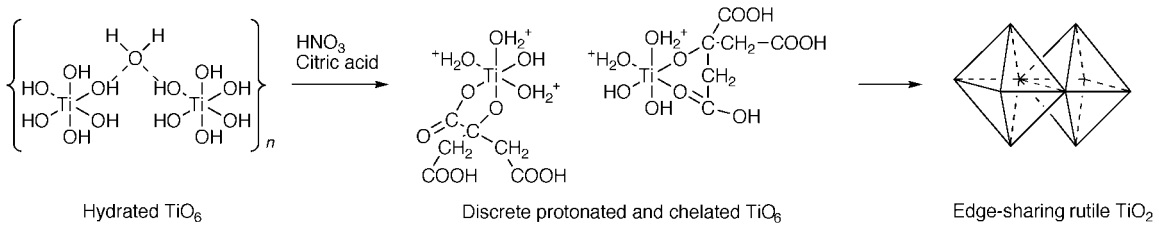

1. Nucleation process of rutile TiO_2 from amorphous phase

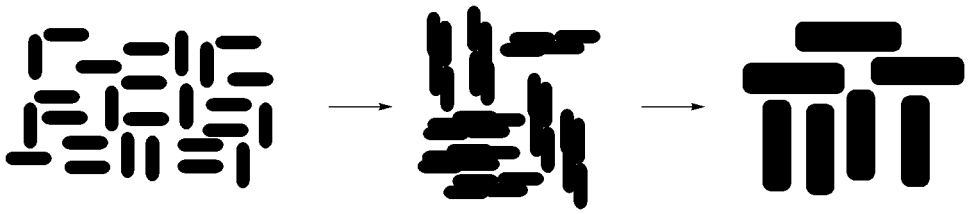

2. Crystal growth by oriented coalescence of primary particles

Scheme 2

Photocatalytic characteristics

The results of photocatalytic oxidation of 2-propanol to acetone by the synthesized anatase and rutile TiO_2 nanocrystallites are shown in Table 3. It is evident that the anatase crystallites (A8) with regular crystal surfaces had a higher photocatalytic activity than that (A12) with irregular crystal surfaces. Prolonging the autoclaving time in the hydrothermal treatment also enhanced the photocatalytic activity of the resulting anatase sample (A8) compared to that (A5) with a shorter autoclaving time. Increasing the autoclaving time should promote the formation of the anatase nanocrystallites with regular crystal surfaces. The anatase TiO_2 nanocrystallites with regular crystal surfaces should have less surface defects, giving highly efficient photocatalysis by suppression of electron–hole pair recombination. On the other hand, the results of the photooxidation of 2-propanol with the different-sized rutile TiO_2 nanocrystallites showed that the photocatalytic activity increased with the decrease of the particle size. Rutile nanocrystallites growing *via* coalescence may have many defects at the interfaces of the coalesced particles.

Conclusions

In the hydrothermal synthesis of TiO_2 nanocrystallites starting from amorphous TiO_2 aggregates, acid catalysis using HF, HCl, and HNO_3 as cooperative acid catalysts leads to the phase-pure formation of anatase TiO_2 nanocrystallites with a narrow size distribution. The effect of protonation prevails in the nucleation and crystal growth when HF is used as an acid catalyst. The chloride or nitrate anions contribute to the nucleation of the anatase from the TiO_6 octahedral species from the starting amorphous aggregates when HCl or HNO_3 is used as a cooperative acid catalyst with HF. The nucleophilicity of the chloride anion should be responsible for the favorable dissolution–precipitation mechanism in the anatase crystal growth from the amorphous phase.

Phase-pure rutile TiO_2 nanocrystallites with rod-like morphology can be synthesized using amorphous TiO_2 as the starting material by chelating and protonating with citric and nitric acids, respectively. The rutile nanocrystal size is readily controlled by changing the pH of the reaction solution, the autoclaving time and the temperature. Acid catalyzes rutile crystal growth from the dissolved TiO_6 octahedra interacting with citric acid molecules, and the coalescence process of neighboring small crystal embryos proceeds as another crystal growth route.

Anatase nanocrystallites with regular crystal surfaces exhibit a higher photocatalytic activity for the oxidation of 2-propanol to acetone than those with irregular surfaces. The photocatalytic activity of the rutile nanocrystallites depends on the particle size. The anatase crystallites possess slightly higher photocatalytic activity for the oxidation of 2-propanol than rutile crystallites.

Acknowledgements

The authors thank Masahiro Oasawa, Sadahiro Iida, and Nobumitu Oshimura (Central Research Laboratory, Sumitomo Metal Mining Co., LTD.) very much for kindly supporting TEM measurements of the TiO_2 samples. This work was financially supported by "Research for the Future" Program, JSPS #96P00305.

References

1 M. A. Fox and M. T. Dulay, *Chem. Rev.*, 1993, **93**, 341.
2 T. Moritz, J. Reiss, K. Diesner, D. Su and A. Chemseddine, *J. Phys. Chem. B*, 1997, **101**, 8052.
3 A. Sclafani and J. M. Herrman, *J. Phys. Chem.*, 1996, **100**, 13655.
4 C. Kormann, D. W. Bahnemann and M. R. Hoffmann, *J. Phys. Chem.*, 1988, **92**, 5196.
5 D. D. Beck and R. W. Siegel, *J. Mater. Res.*, 1992, **7**, 2840.
6 T. Ohno, D. Haga, K. Fujihara, K. Kaizaki and M. Matsumura, *J. Phys. Chem. B*, 1997, **101**, 6415.
7 K. Yanagisawa and J. Ovenstone, *J. Phys. Chem. B*, 1999, **103**, 7781.
8 H. Cheng, J. Ma, Z. Zhao and L. Qi, *Chem. Mater.*, 1995, **7**, 663.
9 J. Moser and M. Grätzel, *J. Am. Chem. Soc.*, 1983, **105**, 6547.
10 M. Anpo, T. Shima, S. Kodama and Y. Kubokawa, *J. Phys. Chem.*, 1987, **91**, 4305.
11 S. -J. Kim, S. -D. Park, Y. H. Jeong and S. Park, *J. Am. Ceram. Soc.*, 1999, **82**, 927.
12 Z. Zhang, C.-C. Wang, R. Zakaria and J. Y. Ying, *J. Phys. Chem. B*, 1998, **102**, 10871.
13 H. Uchida, S. Hirao, T. Torimoto, S. Kuwabata, T. Sakata, H. Mori and H. Yoneyama, *Langmuir*, 1995, **11**, 3725.
14 Y. Zu, X. Li and Z. Wei, *J. Northwest University (Chinese)*, 1998, **28**, 51.
15 X. Ding, Z. Qi and Y. He, *J. Mater. Sci. Lett.*, 1995, **14**, 21.
16 S. Nishimoto, B. Ohtani, H. Kajiwara and T. Kagiya, *J. Chem. Soc., Faraday Trans. 1*, 1985, **81**, 61.

17 I. Moriguchi, H. Maeda, Y. Teraoka and S. Kagawa, *Chem. Mater.*, 1997, **9**, 1050.
18 C.-C. Wang and J. Y. Ying, *Chem. Mater.*, 1999, **11**, 3113.
19 E. Stathatos, P. Lianos, F. Del Monte, D. Levy and D. Tsiourvas, *Langmuir*, 1997, **13**, 4295.
20 S. T. Martin, H. Herrmann and M. R. Hoffmann, *J. Chem. Soc., Faraday Trans.*, 1994, **90**, 3323.
21 Z. Yuan and L. Zhang, *Nanostruct. Mater.*, 1998, **10**, 1127.
22 S. T. Aruna, S. Tirosh and A. Zaban, *J. Mater. Chem.*, 2000, **10**, 2388.
23 Ishihara Sangyo Kaisha Ltd., *Jpn. Kokai Tokkyo Koho*, No. 06-293519, 1994
24 S. Music, M. Gotic, M. Ivanda, S. Popvic, A. Turkovic, R. Trojko, A. Sekulic and K. Furic, *Mater. Sci. Eng. B*, 1997, **47**, 33.
25 C. J. Barbé, F. Arendse, P. Comte, M. Jirousek, F. Lenzmann, V. Shklover and M. Grätzel, *J. Am. Ceram. Soc.*, 1997, **80**, 3157.
26 T. Hirai, H. Sato and I. Komasawa, *Ind. Eng. Chem. Res.*, 1993, **32**, 3014.
27 J.-D. Tsay and T. -T. Fang, *J. Am. Ceram. Soc.*, 1999, **82**, 1409.
28 Y. Wada, K. Tomita, K. Murakoshi and S. Yanagida, *J. Chem. Res. (S)*, 1996, 320.
29 D. Bahnemann, A. Henglein and L. Spanhel, *Faraday Discuss. Chem. Soc.*, 1984, **78**, 151.
30 C. J. Brinker and G. W. Scherer, in *Sol–Gel Science: The Physics and Chemistry of Sol–Gel Processing*; Academic Press, New York, 1990, p. 240.